Fluorescent labelling and biodistribution of latex nanoparticles formed by surfactant-free RAFT emulsion polymerisation

Cheuk Ka Poon[1], Owen Tang[2], Xin-Ming Chen[2], Byung Kim[1], Matthias Hartlieb,[3] Carol A. Pollock[2], Brian S. Hawkett*[1], Sébastien Perrier*[1,3]

[1] *Key Centre for Polymers & Colloids, School of Chemistry, Building F11, The University of Sydney, NSW 2006, Australia*

[2] *Kolling Institute of Medical Research, Royal North Shore Hospital and The University of Sydney, St Leonards, NSW 2065, Australia*

[3] *Department of Chemistry, The University of Warwick, Coventry, CV4 7AL, UK*

Brian.hawkett@sydney.edu.au; s.perrier@warwick.ac.uk

TOC

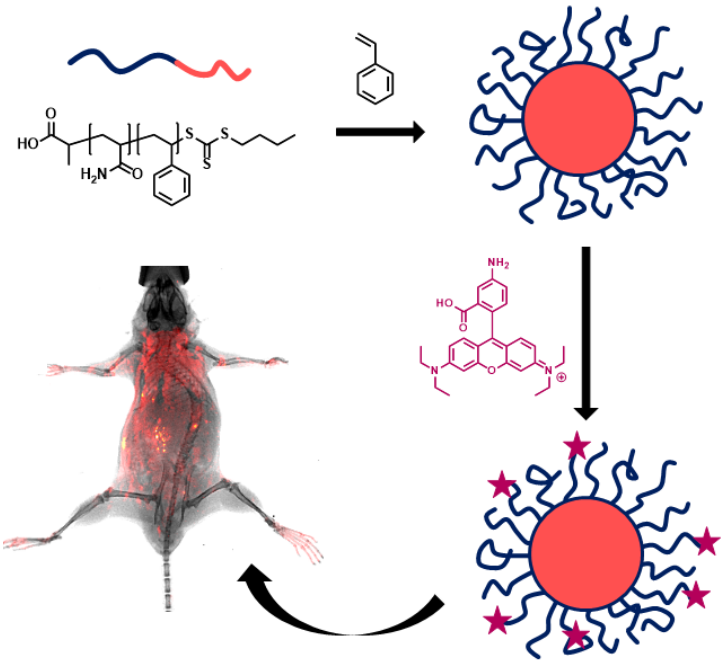

The synthesis and labelling of acrylamide stabilized latex nanoparticles is shown. Particle preparation was performed using surfactant-free RAFT emulsion polymerisation. Labelling was achieved covalently by amidation with rhodamine B amine. Particle tracing was enabled by labelling the sterically stabilised latex particles chemically with rhodamine B. The biodistribution was investigated *in vitro* and *in vivo*.

Abstract

We report the preparation of a novel range of functional polyacrylamide stabilised polystyrene nanoparticles, obtained by surfactant-free reversible addition-fragmentation chain transfer (RAFT) emulsion polymerisation, their fluorescent tagging, cellular uptake and biodistribution. We show the versatility of the RAFT emulsion process for the design of functional nanoparticles of well-defined size that can be used as drug delivery vectors. Functionalisation with a fluorescent tag offers a useful visualisation tool for tracing, localisation and clearance studies of these carriers in biological models. The studies were carried out by labelling the sterically stabilised latex particles chemically with rhodamine B. The fluorescent particles were incubated in a healthy human renal proximal tubular cell line model, and intravenously injected into a mouse model. Cellular localisation and biodistribution of these particles on the biological models were explored.

Introduction

Polymeric nanoparticles are of paramount importance in the field of nanomedicine. Nanoparticles are able to protect their payload from degradation or undesired interaction,[1] solubilize drugs to enable administration or increase the possible dosage,[2] or induce selectivity by passive (*e.g.* enhanced permeability and retention (EPR) effect)[3] or active (*e.g.* by attachment of antibodies,[4] sugars[5] or peptides)[6] targeting. Such systems can be synthesized by a large number of different methods starting either from a polymeric precursor (*e.g.* nanoprecipitation, solvent switch) or directly from monomers (emulsion polymerisation methods).[7] Surfactant-free reversible addition−fragmentation chain transfer (RAFT) emulsion polymerisation displays a particularly valuable method in a biomedical context, as no

surfactants are required to stabilize the formed nanoparticles.[8-10] Hence no molecules can desorb from the particle surface and cause unwanted side-effects or destabilize the colloidal particles.[11] The synthesis is utilized *via* the use of chain transfer agent (CTA)-end-capped diblock copolymers in emulsion.[12-16] The diblock is dispersed in a micellar manner and chain extended with a hydrophobic monomer to form nanoparticles. The potential of these systems in a biomedical context was already demonstrated by Stenzel *et al.* for the production of bacteria interactive particle systems,[17] or by Wang *et al.* with redox responsive particels.[18] We have previously demonstrated the successful conjugation of microRNA (miRNA) duplex to sterically stabilised latex particles formed by surfactant-free RAFT emulsion polymerisation.[19] Fluorescence imaging is a popular non-invasive visualisation technique for biological tracing, diagnosis, detection/sensing and localisation studies *in vitro*, *in vivo* and *ex vivo*.[20-23] Owing to their high sensitivity, versatility and the increasing need to develop next-generation nanomedicines, fluorescent labels are widely incorporated into drug delivery vectors for monitoring the cellular uptake,[24] biodistribution[25] and clearance[26] of the carriers in biological models.

Iron oxide, silica and polymeric particles are common examples of carriers that can be visualised in biological environments with the appropriate fluorescent labelling. For instance, Rosseinsky *et al.* demonstrated the targeting of epithelial cell adhesion molecule (EPCAM) receptor on a human pancreatic cancer cell line with rhodamine-labelled EPCAM-iron oxide nanoparticle conjugates.[27] Zhang *et al.* studied the *in vivo* biodistribution and excretion route of surface-modified silica nanoparticles doped with tris(2,2-bipyridyl) dichlororuthenium (II) hexahydrate (RuBPY) in mice.[28] Likewise, poly(ethylene glycol)-terminated silica nanoparticles tagged with RuBPY dye have been demonstrated to transport across the blood brain barrier *in vitro* and *in vivo* by the group of Yang.[29] Polystyrene beads loaded with

oxygen-sensitive platinum(II) meso-tetrakis-(pentafluorophenyl)-porphyrinato-complex dye were used for intracellular oxygen content sensing in epithelial normal rat kidney cell line.[30]

Rhodamine labels possess a number of attractive physical properties for biological imaging because of their high water-solubility, large extinction coefficient in aqueous solution, high quantum yield, tolerance to photobleaching, relatively long fluorescence lifetime,[31] as well as emission in the visible light region.[32]

Herein, we demonstrate the synthesis of latex nanoparticles by surfactant free RAFT emulsion polymerisation. Particles were synthesized in two different sizes (11 and 22 nm) by variation of the monomer to macro-CTA ratio. Free carboxylic acid functions on the particle surface were used to attach rhodamine as a fluorescent label in order to examine the cellular uptake and *in vivo* bio-distribution (Scheme 1). In vitro cellular uptake was investigated using the human renal proximal tubular cell line (HK2) model for uptake and localisation studies through fluorescent live-cell imaging. HK2 cells were used as models in light of our previous study on miRNA delivery to HK2 cells by nanoparticles, as a mean to decrease the production of fibronectin, which plays a key role in the development of renal fibrosis.[19] Using *in vivo* fluorescent imaging, bio-distribution of 22 nm labelled particles was probed using a mouse model and the accumulation of these fluorescent particles in mouse organs was then examined *via ex vivo* imaging.

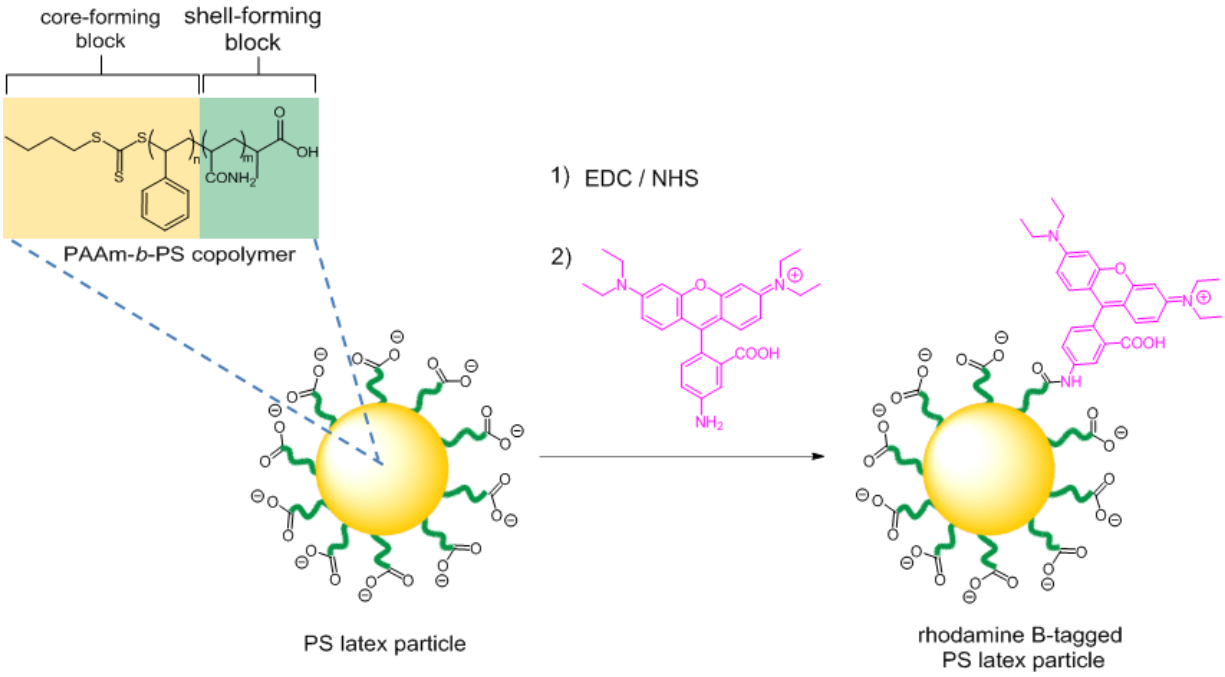

Scheme 1. Conjugation of rhodamine B-amine to PS latex particles.

Results and discussion

Synthesis of poly(acrylamide) stabilized latex nanoparticles

The synthesis of poly(acrylamide) (PAAm) stabilized poly(styrene) (PS) nanoparticles was carried out by surfactant free RAFT emulsion polymerisation using a macro-CTA. This amphiphilic diblock copolymer consisting of PAAm as a water soluble block and PS as selective block was produced by RAFT polymerisation. Acrylamide (AAm) was polymerized in a water-dioxane solvent mixture (60/40 v/v) using 2-propanoyl butyl trithiocarbonate (PABTC) as chain transfer agent. The carboxylic acid located on the R groups of the CTA was necessary for stabilization of latex particles, as well as for later attachment of the dye. Conversion (93%) and degree of polymerisation (DP = 14) were determined by ^{1}H-NMR spectroscopy comparing signals of the polymer backbone with vinyl peaks of the monomer or the methyl peak of the CTA Z-group, respectively (Figure S1). ESI mass spectrometry shows a main distribution of the desired PAAm homopolymer bearing R group and trithiocarbonate

Z-group of the RAFT agent (Figure S2). A small doubly charged distribution could be attributed to the termination product as a result of the combination of two growing chains. Block extension was attempted without purification by addition of styrene in a dioxane/water mixture, thus altering the solvent ration to (70/30 v/v). After polymerisation monomer conversion was found to be 90 % resulting in a DP of 8 for the PS block (Figure S3). Due to poor solubility of the RAFT agent ESI-MS as well as size exclusion chromatography could not be performed.

In order to utilize the produced macro-CTA for RAFT emulsion polymerisation, micellisation was induced by a change in the solvent ratio of the polymerisation mixture. The non-purified polymerisation solution of $PAAm_{14}$-b-PS_8 was, therefore, diluted with water in the presence of NaOH. The base was required to deprotonate the carboxylic acid on the R-group of the polymer leading to an enhanced stabilization of the micelles by the anionic charges on the corona. It should be noted, that the trithiocarbonate, which might be hydrolysed under alkaline conditions is located at the PS chain end within the core compartment of the micelle, leading to a protection of the CTA. A diameter of 9.3 nm with a PDI of 0.216 was measured using Dynamic light scattering (DLS).

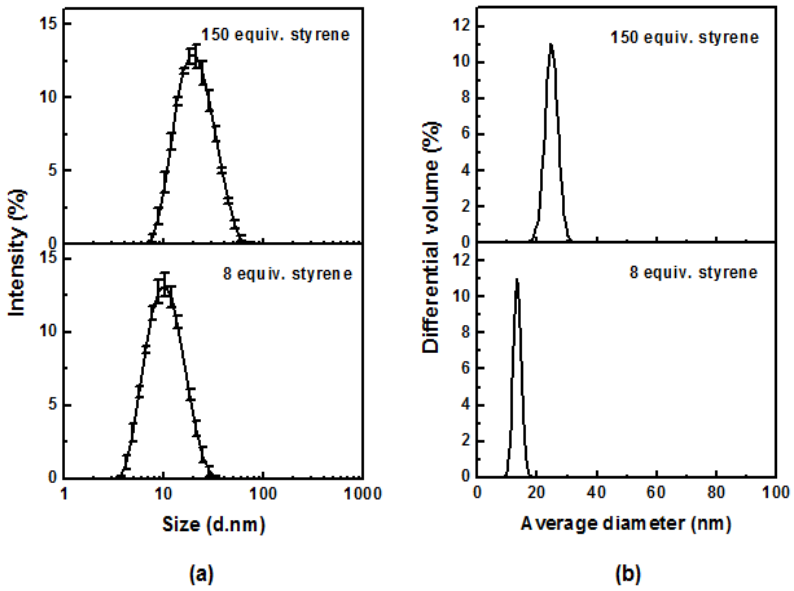

Figure 1. PS latex particles size distributions measured from (a) DLS $_{intensity}$ and (b) HDC.

In order to form nanoparticles, styrene was added to the solution of macro CTA micelles and dispersed by stirring. After the mixture became homogeneous, radical initiator, as well as a further portion NaOH, to ensure colloidal stability, was added. The polymerisation was performed at elevated temperature until the reaction solution became clear. This observation indicates a consumption of styrene from the dispersion and the formation of PAAm stabilized nanoparticles. Using different monomer to macro-CTA ratios (8:1 and 150:1, respectively) the final size of the nanoparticles was varied. In the case of 8:1 monomer CTA ratio, 99% of monomer conversion was achieved and resulting particles were studied by DLS (d = 11 nm, PDI = 0.159) and hydrodynamic chromatography (HDC) (d = 13 nm) (Figure 1, Table 1). Increased styrene content lead to the formation of particles with a diameter of 22 nm (DLS) and 25 nm (HDC), respectively at a monomer conversion of 72%. Both nanoparticle solutions were purified by dialysis and investigated by transmission electron microscopy (TEM) resulting in similar size values to those obtained by scattering and chromatography (Figure 2).

The slightly decreased diameter detected by TEM can be explained by the collapse of the stabilizing polyacrylamide chains onto the particle surface when the particles were dried down on the TEM grid.

Table 1: Characterization data of polymeric precursors and polymers constituting latex nanoparticles.

Sample	NMR				DLS		HDC		TEM	Labelling efficiency (%)
	DP (AAm)	DP (S)	Mn	Conversion	Size (d, nm)	PDI	Size (d, nm)	CV	Size (d, nm)	
P(AAm)	14	-	1,200	93	-	-	-	-	-	-
Macro-CTA	14	8	2,100	90	9.3	0.216	-	-	-	-
NP 11 nm	14	16	2,900	99	11	0.159	13	10	7.5	10
NP 22 nm	14	116	13,300	72	22	0.167	25	9	17	12

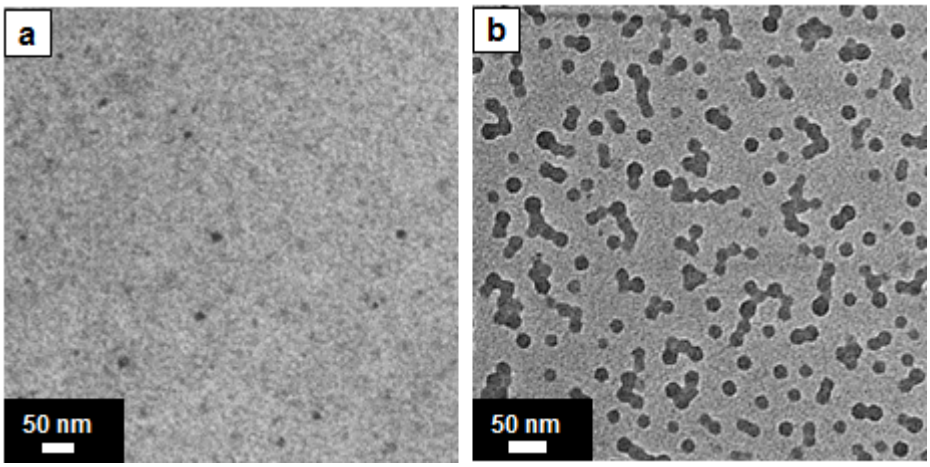

Figure 2. TEM images of PS latex particles synthesised from RAFT emulsion polymerisation after dialysis. Styrene monomer fed relative to macro-RAFT: (a) 8 equivalents, (b) 150 equivalents.

Fluorescence labelling of latex nanoparticles

The synthesis of the rhodamine-PS latex particle conjugate was carried out in two steps: 1) The preparation of rhodamine B amine by the hydrolysis of rhodamine isothiocyanate; 2) The conjugation of rhodamine B amine to the carboxylic acids on the ends of the stabilizer chains *via* EDC/NHS coupling.

In order to synthesize an amine functional rhodamine derivative, commercially available rhodamine B isothiocyanate (RBITC) was hydrolysed in an aqueous environment. The dye was hydrolysed in water over night and the reaction was monitored by ESI mass spectrometry (Figure 3). Addition of water resulted in the formation of a thiocarbamate, which reacted into the amine by elimination of cabonylsulfide (Scheme S1).[33,34] Absence of a peak at m/z 500 indicated the complete hydrolysis of the isothiocyanate. The presence of the dimeric derivative is a result of the reaction of isothiocyanate moieties with already hydrolysed dye.

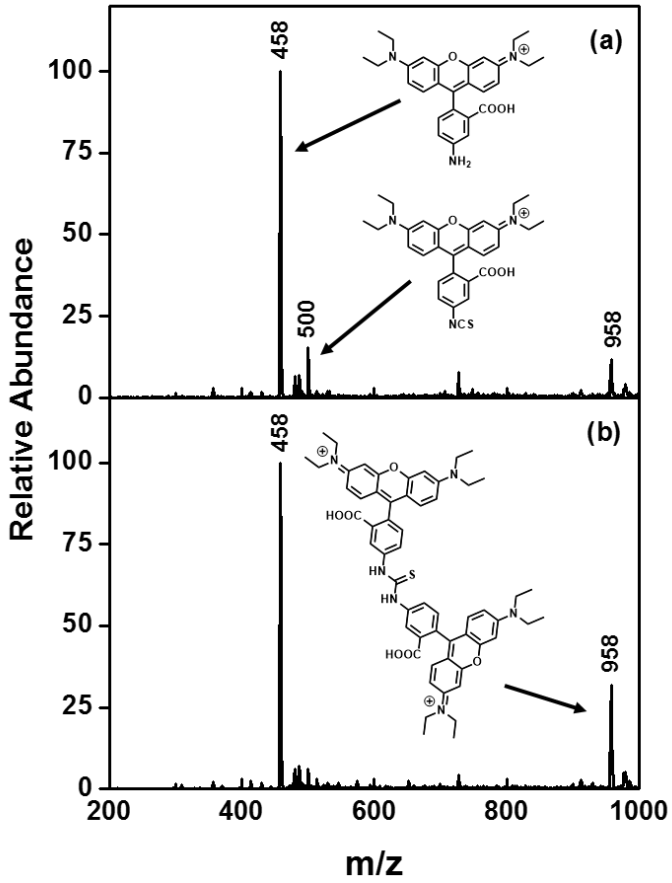

Figure 3. ESI-MS of RBITC (a) before and (b) after hydrolysis reaction. Signals at 458 m/z, 500 m/z correspond to the amine and isothiocyanate derivatives of rhodamine B, respectively. Signal at 958 m/z represents thiourea-linked rhodamine dimer.

Rhodamine B amine was, subsequently, used for labelling the PS latex particles. Aiming to functionalize 10% of functional groups on the ends of the stabilizer chains with the fluorescent dyes, carboxylic acid groups were first activated by 12 equivalents EDC and 25 equivalents NHS per carboxylic acid for 60 minutes. As the shell of the particles is densely populated with carboxyl groups and, therefore, highly charged a large excess of activation reagents was used to ensure (partial) activation. Subsequently, the reaction mixture was added to the aqueous rhodamine B amine solution. A 30% excess of the rhodamine dye was supplied for the reaction to compensate for the presence of thiourea-linked rhodamine dimer resulted from RBITC hydrolysis. After purification by dialysis, the rhodamine-tagged particles were characterised by UV-Vis and fluorescence spectroscopy. The characteristics absorption peak at 310 nm in Figure 4Figure 4 corresponds to the trithiocarbonate group of the CTA of PS latex particles.[35]

Absorbance of the rhodamine B of labelled nanoparticles was observed at 562 nm. The signal shows a red shift of 10 nm as compared to the free dye (Figure 4). The particles exhibit a maximum fluorescence excitation and emission wavelengths at 562 nm and 583 nm, respectively (Figure 5). The observed wavelengths also exhibited a bathochromic shift of 11 nm from the maximum excitation and emission of the free dye. The shifts of absorption and fluorescence spectra were attributed to a change in the fluorophore chemical structure and chemical environment surrounding the fluorophore, which were strong evidence for attachment of dye molecules to the particles.[36-38] The amount of rhodamine dye loaded onto the PS latex particles was determined using the Beer-Lambert law with the pre-determined extinction coefficient (ε) of the free dye in water (ε = 40400 $M^{-1} \cdot cm^{-1}$ at 552 nm, (Figure S4) and known particle concentration. The conjugation efficiencies for the 11 nm and 22 nm particles were found to be 10% and 12%, respectively in regard to the total amount of carboxyl groups on the particle surface (see Supporting Information for calculation). These

are equivalent to attaching 10 and 14 rhodamine molecules to the 11 nm and 22 nm particles correspondingly.

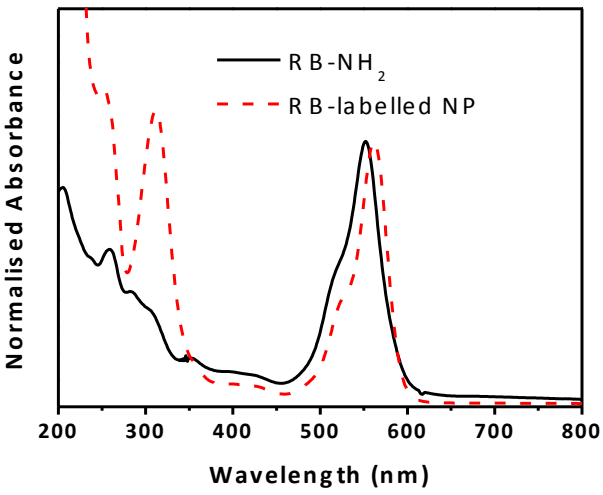

Figure 4. Example UV-Vis absorption spectra of rhodamine B amine (RB-NH_2) and rhodamine-tagged particles (RB-labelled NP) in water.

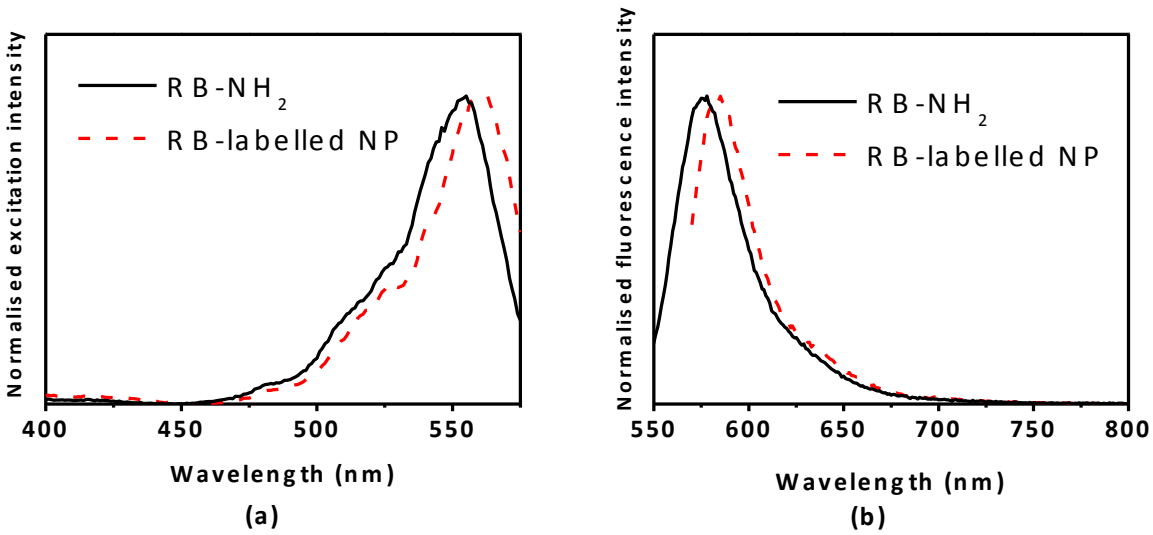

Figure 5. Example fluorescence (a) excitation and (b) emission spectra of free rhodamine B amine (RB-NH_2) and rhodamine-tagged PS latex particles (RB-labelled NP).

Cellular uptake of rhodamine-tagged PS latex particles. Human renal proximal tubular cells (HK2) were chosen as the model cell line for studying the nanoparticle uptake *in vitro*. The cellular uptake of the rhodamine-labelled particles was observed by confocal microscopy. HK2 cells were incubated with the fluorescent particles for 24 hours before imaging. The nuclei of the cells were stained with blue fluorescent 4',6-diamidino-2-phenylindole (DAPI) and Hoechst dyes for visualising the uptake of 11 nm and 22 nm particles, respectively. HK2 cells without dosing with rhodamine-tagged particles were used as the negative control for the studies. Confocal images of HK2 cells dosed with 11 nm and 22 nm rhodamine-tagged particles are shown in Figure and Figure correspondingly. Cellular uptake of particles is evident from the red fluorescence within the boundaries of the cellular membrane as shown by comparison of reflexion image and the red fluorescence channel in the merged pictures. The particles were found inside the vesicular structures of the cells, implying that they were internalised and taken up by the cells during the 24 hour incubation. The punctuate structure of the red fluorescence signals in the rhodamine channel indicates a lysosomal or endosomal colocalization. As nanoparticle system in this size range is predominantly uptaken *via* endocytosis, this would be in agreement with their localization.[39,40] The intracellular and presumable cytoplasmic localisation suggest the particles can be used for the intracellular delivery of mature miRNA, which can only be processed into RNA-induced silencing complexes (RISC) in the cytoplasm for targeting the corresponding messenger RNA (mRNA).[41] For such application, the nanoparticles would only be required to cross the cellular membrane to reach the target site, without the need to cross the nuclei barrier. The reversible covalent decoration of such particles using miRNA was previously described by our group.[19]

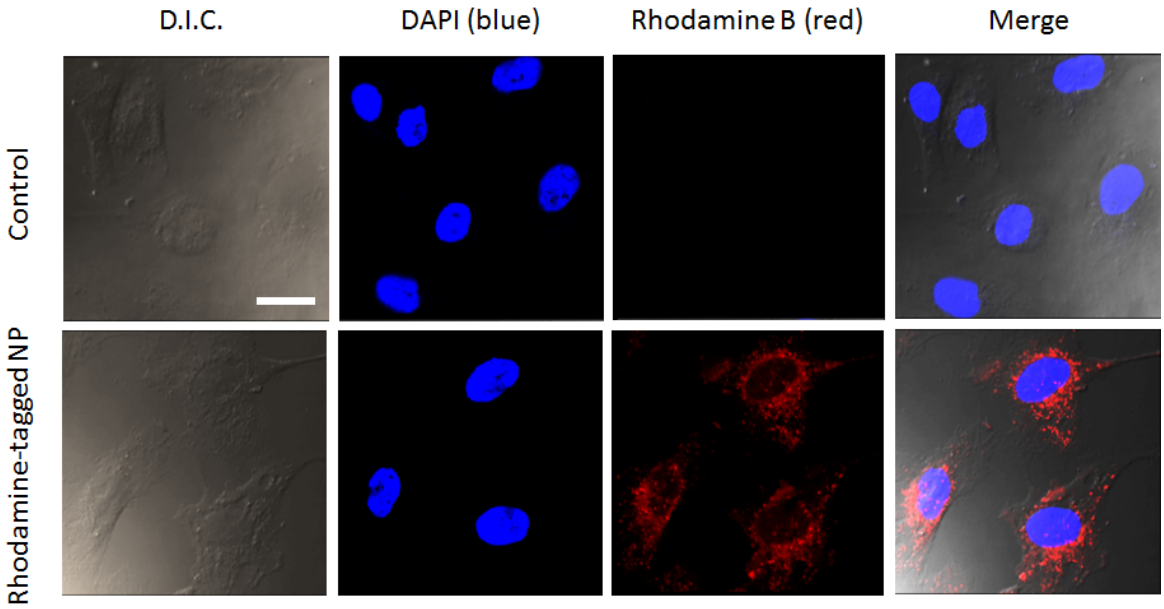

Figure 6. Confocal images of HK2 cells dosed with 22 nm rhodamine-tagged PS latex particles (red fluorescence). The cell nuclei were stained with DAPI (blue fluorescence). Scale bar = 25 μm.

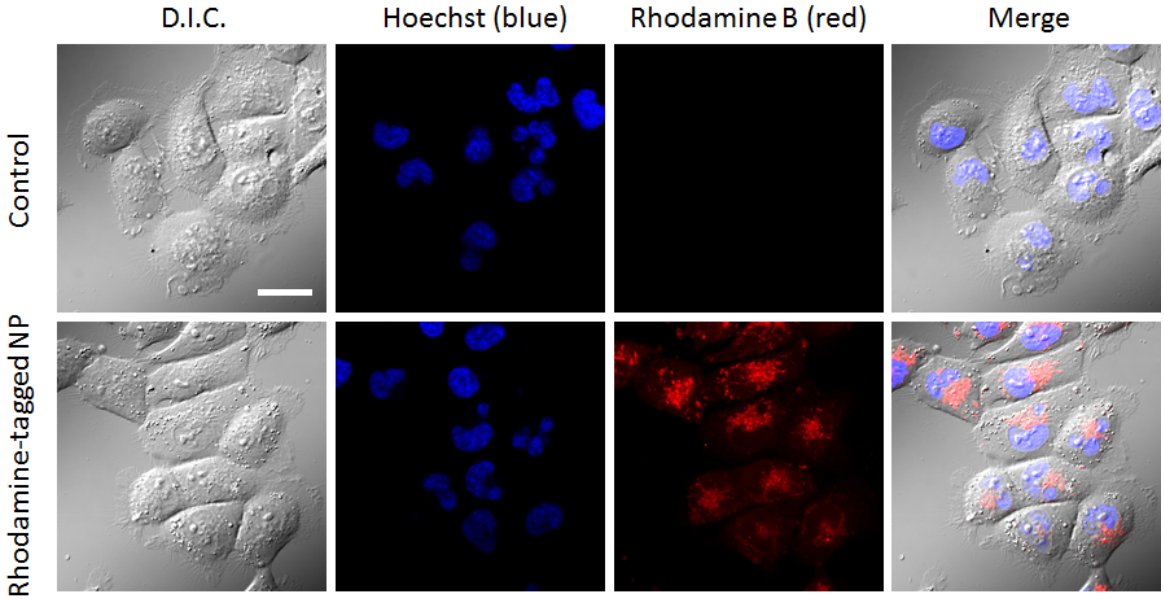

Figure 7. Confocal images of HK2 cells dosed with 11 nm rhodamine-tagged PS latex particles (red fluorescence). The cell nuclei were stained with Hoechst (blue fluorescence). Scale bar = 25 μm.

In vivo and ex vivo biodistribution of rhodamine-labelled PS latex particles.

The biodistribution of rhodamine-tagged PS latex particles was studied in healthy mice as biological models. The 22 nm particles were selected for the investigation. Following intravenous administration of the 22 nm rhodamine-labelled particles, the mouse model was exposed for fluorescence imaging for the detection of rhodamine signals *in vivo*. Figure c reveals that red fluorescence was emitted from the vasculature of the mouse torso and limbs, suggesting the rhodamine-tagged particles have been administered into the bloodstream and were transported through the cardiovascular system. The mouse was anatomised for *ex vivo* studies 40 minutes after dosing with the fluorescent particles. The heart, lungs, liver and kidneys were dissected from the mouse and their fluorescence images were collected. All the dissected organs emitted rhodamine fluorescence signals (Set II in Figure b and Figure c) as opposed to the organs obtained from the negative control mouse (without particle injection, Set I in Figure b and Figure c). The fluorescence indicated that the rhodamine-tagged particles had been distributed to the major organs through blood circulation. Accumulation of the fluorescent particles appeared to be highest in the liver, which showed the strongest fluorescence intensity. The lungs also exhibited a prominent uptake of the fluorescent particles, followed by the kidneys and the heart. Since more than 50% of the cardiac blood output is received by the lung vasculature, depositions of particles there was anticipated as the particles were transported through the mouse bloodstream *via* intravenous administration.[42] The high accumulation of particles in the lungs could be explained by the extensive capillary network covering the pulmonary alveoli, which contain fine structures of capillaries with diameter ranging between 1 μm and 5 μm. The particles were expected to be transported slower in these capillaries than in other blood vessels, thereby being retained in the organ.[42] The heavy deposition of particles in the liver might indicate their possible elimination by the

liver Kupffer cells through the reticuloendothelial system (RES), which could be associated with systemic administration of the nanoparticles.[43-45]

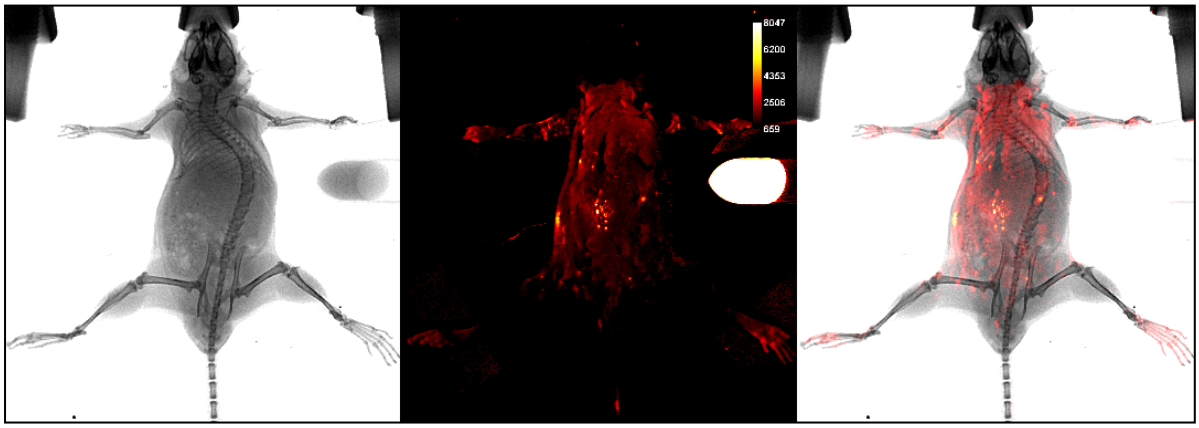

Figure 8. *In vivo* images of the mouse model after intravenous injection of 22 nm rhodamine-labelled PS latex particles. Biodistribution of the particles (red fluorescence) was studied by imaging the mouse model with (a) X-ray (b) fluorescence and (c) X-ray/fluorescence overlay modes. An eppendorf tube containing the 22 nm rhodamine-tagged latex particles before injection was placed next to the mouse model for comparing with the fluorescence intensity of particles *in vivo*.

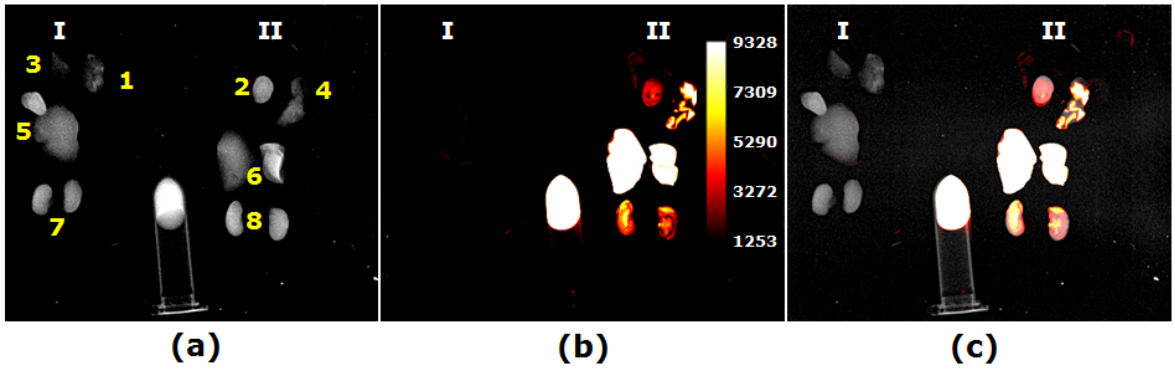

Figure 9. *Ex vivo* images of different organs collected from the mice (I) without (negative control) and (II) after intravenous injection with 22 nm rhodamine-labelled PS latex particles. Organs dissected from the mice were visualised by (a) X-ray, (b) fluorescence and (c) X-

ray/fluorescence overlay modes. An eppendorf tube containing the 22 nm rhodamine-tagged latex particles before *in vivo* injection was used for comparing with the fluorescence intensity of the organs: (1-2) Heart, (3-4) lungs, (5-6) liver, (7-8) kidneys.

Conclusions

Poly(acrylamide) stabilized nanoparticles were produced by surfactant free RAFT emulsion polymerisation. The size of the colloids was controlled by the ratio of monomer to macro-CTA in emulsion, resulting in nanoparticles with 11 and 22 nm diameter respectively. Free carboxylic acid functional groups on the stabilizer chains were used for fluorescence labelling with rhodamine B. For this purpose, the commercially available isothiocyanate functionalized dye was hydrolysed in an aqueous environment to yield rhodamine B with primary amine functions. Attachment was utilized using EDC/NHS coupling and resulted in the functionalization of 10% and 12% of the available functional groups for the 11 and 22 nm particles, respectively. This corresponded to 10 and 14 dye molecules per particle.

The rhodamine-labelled PS latex particles were used to monitor the cellular uptake and biodistribution *in vitro* and *in vivo*. Both 11 nm and 22 nm fluorescent particles were taken up by HK2 cells and localised in the cytoplasm after 24 hours of incubation. The cytoplasm can be the target site for the nanoparticles for potential applications in the intracellular delivery of miRNA, which could only be processed into RISC in the cytoplasm for mRNA targeting.

For *in vivo* studies, the 22 nm rhodamine-tagged particles were intravenously injected into a mouse model systemically and were found to transport through the vasculature of the mouse torso and limbs. *Ex vivo* studies revealed that the fluorescent particles were distributed predominantly in the mouse liver, followed by the lungs, kidneys and the heart. Pulmonary

retention of the particles could possibly be due to slow transportation by the small capillaries present in the alveolar vasculature.

Acknowledgements

The authors wish to thank Australian Centre for Microscopy & Microanalysis (confocal microscope) for instrumental support. The University of Sydney is gratefully acknowledged for funding. MH gratefully acknowledges the German Research Foundation (DFG, GZ: HA 7725/1-1) for funding. BK gratefully acknowledges Sirtex Technology for funding.

Experimental

Materials for the synthesis of rhodamine-labelled PS latex particles. PAAm stabilised PS latex particles (11 nm and 22 nm) were synthesised according to protocol described in Supporting Information. Rhodamine B isothiocyanate (RBITC, mixed isomers, Sigma-Aldrich), *N*-(3-dimethylaminopropyl)-*N*′-ethylcarbodiimide hydrochloride (EDC, 98+%, purum, Sigma-Aldrich), *N*-hydroxysuccinimide (NHS, 99.8%, Sigma-Aldrich), methanol for ESI-MS (MeOH, 99.80%, HPLC grade, Merck), were used as received. Water was purified by Milli-Q® Integral Water Purification System (resistivity of water = 18.2 MΩ · cm at 25°C). 2-(*N*-Morpholino)ethanesulfonic acid (MES, 99+%, Sigma-Aldrich) buffer stock solution (100 mM, pH 5.65) was prepared with Milli-Q water and the pH was adjusted with aqueous NaOH (100 mM).

Electrospray ionisation mass spectrometry (ESI-MS). Rhodamine dyes were characterised on mass spectrometer (Finnigan™ LCQ™ Deca), using MeOH (HPLC grade) as the eluent at a

flow rate of 0.2-0.4 mL/min and nitrogen as the sheath gas, with the electrospray voltage set at 4.5 kV and capillary temperature at 300 °C. Samples were diluted to a final concentration of ~ 0.1 mg/mL and filtered through 0.20 μm membrane before injection.

Ultraviolet-visible (UV-Vis) spectrometry. UV-Vis absorbance of the rhodamine-labelled PS latex particles and free rhodamine B amine were measured using UV-Vis-NIR spectrometer (Varian Cary 5000, Agilent). Measurements were taken in the range of 260-800 nm at 600 nm/min.

Preparation of UV-Vis calibration curve of rhodamine B amine. Aqueous rhodamine B amine solution prepared was diluted with water to different concentrations in the range of 3-37 μM. The absorbance values of the rhodamine B amine solutions at 552 nm were collected for the construction of standard curve. Water was used as the blank for the measurement.

Fluorescence spectroscopy. Fluorescence of free and conjugated rhodamine was detected by fluorescence spectrometer (Cary Eclipse, Agilent). Samples were scanned at 600 nm/min, with the excitation and emission slits set at 10 nm width.

Preparation of rhodamine B amine from hydrolysis of rhodamine B isothiocyanate (RBITC). RBITC (0.0050g, 0.0097 mmol) was dissolved in water (25 g) and stirred at room temperature overnight. ESI-MS (m/z): amine derivative of rhodamine B $[C_{28}H_{32}N_3O_3]^+$ = 458; unreacted isothiocyanate derivative of rhodamine B $[C_{29}H_{30}N_3O_3]^+$ = 500.

Typical synthesis of rhodamine-labelled polymeric nanoparticles. 11 nm PS latex (SC = 0.37%, 2.5 mL) was diluted in MES buffer (100 mM, pH 5.65, 2.5 mL), followed by mixing with EDC (0.0183 g, 0.096 mmol) and NHS (0.0227 g, 0.197 mmol) for an hour at room temperature. After the addition of aqueous rhodamine B amine solution (0.4 mM, 2.5 mL,

1.01 μmol), the reaction was kept in the dark and stirred overnight at room temperature (Scheme 1). The rhodamine-conjugated latex particles were purified by dialysis against Milli-Q water (MW cut-off = 2000 g/mol) in the dark. SC of the particles after modification = 0.12%. The absorbance and conjugation efficiency of the rhodamine-functionalised particles was checked by UV-Vis spectrometry, using water as the blank for the measurements. Rhodamine fluorescence from the particles was detected by fluorescence spectroscopy.

Cell culture. The cellular uptake of rhodamine-labelled PS latex particles was studied in healthy human renal proximal tubular cell line (HK2, provided by the Renal Research Laboratory, Kolling Institute of Medical Research, the Royal North Shore Hospital). Confluent monolayers of HK2 cells were grown in keratinocyte-serum-free medium (Gibco), which was supplemented with 50 μg/mL bovine pituitary extract (Gibco) and 5 ng/mL recombinant human epidermal growth factor (Gibco). The cells were cultured under humidified conditions at 37 °C with 5% (v/v) CO_2. For sub-culturing, the growth media was removed from the cells, which were then rinsed with phosphate buffer saline (PBS, In vitro Technologies). After the addition of 0.25% (w/v) trypsin (SAFC Biosciences), the cells were detached from the surface and washed with fresh culture medium. The rinsed cells were collected by centrifugation at 1000 g for 3 minutes and transferred to fresh culture medium for incubation.

Cellular uptake of rhodamine-tagged PS latex particles. Rhodamine-labelled latex particles were sterilised by filtering through a 0.22 μm filter. The sterilised particles were diluted with cell culture media to a final concentration of 10 ppm for incubation with HK2 cells for 24 hours. Localisation of the rhodamine-tagged particles in HK2 cells was imaged under confocal microscopy. The nuclei of the HK2 cells were visualised under confocal microscopy by fluorescent staining: HK2 cells dosed with 22 nm rhodamine-tagged particles were

immobilised on glass surface and stained with 4',6-diamidino-2-phenylindole (DAPI, Life Technologies) in mounting media for confocal microscopy overnight before imaging; HK2 cells incubated with 11 nm rhodamine-labelled particles were stained with Hoechst 30 minutes prior to imaging.

Cellular uptake studies of 22 nm rhodamine-tagged PS latex particles. The uptake of the 22 nm rhodamine-labelled particles by HK2 cells was observed under a confocal microscope (TCS SP5, Leica Microsystems). Images were taken with an.63× oil objective, with the numerical aperture set at 1.4. Fluorescence of (DAPI) in the nuclei of HK2 cells was captured between 415 nm and 556 nm by excitation at 405 nm. Rhodamine fluorescence signal in HK2 cells was imaged between 614 nm and 748 nm by excitation at 561 nm.

Cellular uptake studies of 11 nm rhodamine-tagged PS latex particles. The localisation of the 11 nm rhodamine-tagged PS latex particles in HK2 cells was imaged under an inverted confocal microscope (Olympus FV1000). The imaging was performed with a 60× water objective, with the numerical aperture set at 1.2. Fluorescence of Hoechst stain in the nuclei of HK2 cells was collected between 425 nm and 475 nm by excitation at 405 nm. Cellular rhodamine fluorescence was captured between 570 nm and 670 nm by excitation at 559 nm.

Animal model for rhodamine-labelled PS latex particle injection. Animal experiments were approved by the Royal North Shore Hospital Animal Care and Ethics Committee, Australia (Protocol No. 1310-001A). Injection of rhodamine-tagged PS latex particles were performed in 8-week-old healthy male mice (C57BL/6, Kolling Institute of Medical Research, the Royal North Shore Hospital), each weighing around 25 g.

In vivo and *ex vivo* imaging. *In vivo* and *ex vivo* imaging were performed on a preclinical animal imaging system (In-vivo FX PRO, Burker). X-ray and fluorescence detection modes were used for visualising the mouse skeletal features and biodistribution of the rhodamine-tagged particles, respectively. Fluorescence of rhodamine signals was collected at 600 nm by excitation at 550 nm. Fluorescence images were obtained by subtracting the skin auto-fluorescence of the animal models with spectral unmixing, using fluorescence of rhodamine-labelled particles as the control.

In vivo and *ex vivo* studies of 22 nm rhodamine-tagged PS latex particles. The mice were given an inhalational anaesthetic (2% (v/v) isoflurane) prior to nanoparticle administration. 200 μL of rhodamine-labelled latex dispersed in PBS buffer (12.3 ppm) was injected into the lateral veins of the mouse tails. The biodistribution of the fluorescent particles *in vivo* was visualised by a preclinical animal imaging system. Forty minutes after particle injection, the mice were anaesthetised with 2% (v/v) isoflurane and underwent pericardiectomy. The mice were perfused with PBS before organ removal. The fluorescence images of the mouse heart, lungs, liver and kidneys *ex vivo* were collected by preclinical animal imaging system. A healthy mouse without particle injection was also sacrificed for pericardiectomy to serve as the negative control for the *ex vivo* studies.

References

(1) Vrignaud, S.; Benoit, J.-P.; Saulnier, P. *Biomaterials* **2011**, *32*, 8593.

(2) Ma, P.; Mumper, R. J. *Journal of nanomedicine & nanotechnology* **2013**, *4*, 1000164.

(3) Maeda, H.; Greish, K.; Fang, J. In *Polymer Therapeutics II*; Satchi-Fainaro, R., Duncan, R., Eds.; Springer Berlin Heidelberg: 2006; Vol. 193, p 103.

(4) Fay, F.; Scott, C. J. *Immunotherapy* **2011**, *3*, 381.
(5) Zhao, J.; Babiuch, K.; Lu, H.; Dag, A.; Gottschaldt, M.; Stenzel, M. H. *Chemical Communications* **2014**, *50*, 15928.
(6) Ruoslahti, E. *Advanced Materials* **2012**, *24*, 3747.
(7) Rao, J. P.; Geckeler, K. E. *Progress in Polymer Science* **2011**, *36*, 887.
(8) Ferguson, C. J.; Hughes, R. J.; Pham, B. T. T.; Hawkett, B. S.; Gilbert, R. G.; Serelis, A. K.; Such, C. H. *Macromolecules* **2002**, *35*, 9243.
(9) Ferguson, C. J.; Hughes, R. J.; Nguyen, D.; Pham, B. T. T.; Gilbert, R. G.; Serelis, A. K.; Such, C. H.; Hawkett, B. S. *Macromolecules* **2005**, *38*, 2191.
(10) Ganeva, D. E.; Sprong, E.; de Bruyn, H.; Warr, G. G.; Such, C. H.; Hawkett, B. S. *Macromolecules* **2007**, *40*, 6181.
(11) Urbani, C. N.; Monteiro, M. J. In *Handbook of RAFT Polymerisation*; Wiley-VCH Verlag GmbH & Co. KGaA: 2008, p 285.
(12) Chenal, M.; Bouteiller, L.; Rieger, J. *Polymer Chemistry* **2013**, *4*, 752.
(13) Fréal-Saison, S.; Save, M.; Bui, C.; Charleux, B.; Magnet, S. *Macromolecules* **2006**, *39*, 8632.
(14) Pepels, M. P. F.; Holdsworth, C. I.; Pascual, S.; Monteiro, M. J. *Macromolecules* **2010**, *43*, 7565.
(15) Chaduc, I.; Girod, M.; Antoine, R.; Charleux, B.; D'Agosto, F.; Lansalot, M. *Macromolecules* **2012**, *45*, 5881.
(16) Yeole, N.; Hundiwale, D.; Jana, T. *J. Colloid Interface Sci.* **2011**, *354*, 506.
(17) Ting, S. R. S.; Min, E. H.; Zetterlund, P. B.; Stenzel, M. H. *Macromolecules* **2010**, *43*, 5211.
(18) Jiang, G.; Wang, Y.; Zhang, R.; Wang, R.; Wang, X.; Zhang, M.; Sun, X.; Bao, S.; Wang, T.; Wang, S. *ACS Macro Letters* **2012**, *1*, 489.
(19) Poon, C. K.; Tang, O.; Chen, X.-M.; Pham, B. T. T.; Gody, G.; Pollock, C. A.; Hawkett, B. S.; Perrier, S. *Biomacromolecules* **2016**, *17*, 965.
(20) Blow, N. *Nat. Meth.* **2009**, *6*, 465.
(21) Lichtman, J. W.; Conchello, J.-A. *Nat. Meth.* **2005**, *2*, 910.
(22) Giepmans, B. N. G.; Adams, S. R.; Ellisman, M. H.; Tsien, R. Y. *Science* **2006**, *312*, 217.
(23) Leblond, F.; Davis, S. C.; Valdés, P. A.; Pogue, B. W. *J. Photochem. Photobiol. B: Biol* **2010**, *98*, 77.
(24) Fernando, L. P.; Kandel, P. K.; Yu, J.; McNeill, J.; Ackroyd, P. C.; Christensen, K. A. *Biomacromolecules* **2010**, *11*, 2675.
(25) Liu, Y.; Tseng, Y.-c.; Huang, L. *Pharm. Res.* **2012**, *29*, 3273.
(26) Longmire, M.; Choyke, P. L.; Kobayashi, H. *Nanomedicine (London, England)* **2008**, *3*, 703.
(27) Olariu, C. I.; Yiu, H. H. P.; Bouffier, L.; Nedjadi, T.; Costello, E.; Williams, S. R.; Halloran, C. M.; Rosseinsky, M. J. *J. Mater. Chem.* **2011**, *21*, 12650.
(28) He, X.; Nie, H.; Wang, K.; Tan, W.; Wu, X.; Zhang, P. *Anal. Chem.* **2008**, *80*, 9597.
(29) Liu, D.; Lin, B.; Shao, W.; Zhu, Z.; Ji, T.; Yang, C. *ACS Appl. Mater. Interfaces* **2014**, *6*, 2131.
(30) Wang, X.-d.; Gorris, H. H.; Stolwijk, J. A.; Meier, R. J.; Groegel, D. B. M.; Wegener, J.; Wolfbeis, O. S. *Chem. Sci.* **2011**, *2*, 901.
(31) Lavis, L. D.; Raines, R. T. *ACS Chem. Biol.* **2008**, *3*, 142.
(32) Beija, M.; Afonso, C. A. M.; Martinho, J. M. G. *Chem. Soc. Rev.* **2009**, *38*, 2410.
(33) Joseph, V. B.; Satchell, D. P. N.; Satchell, R. S.; Wassef, W. N. *J. Chem. Soc. Perkin Trans. 2* **1992**, 339.

(34) Pecháček, R.; Velíšek, J.; Hrabcová, H. *J. Agric. Food Chem.* **1997**, *45*, 4584.
(35) Skrabania, K.; Miasnikova, A.; Bivigou-Koumba, A. M.; Zehm, D.; Laschewsky, A. *Polym. Chem.* **2011**, *2*, 2074.
(36) Nguyen, T.; Francis, M. B. *Org. Lett.* **2003**, *5*, 3245.
(37) Roy, B. C.; Peterson, R.; Mallik, S.; Campiglia, A. D. *J. Org. Chem.* **2000**, *65*, 3644.
(38) Puvvada, N.; Mandal, D.; Panigrahi, P. K.; Pathak, A. *Toxicol. Res.* **2012**, *1*, 196.
(39) Xiang, S.; Tong, H.; Shi, Q.; Fernandes, J. C.; Jin, T.; Dai, K.; Zhang, X. *J. Control. Release* **2012**, *158*, 371.
(40) Oh, N.; Park, J.-H. *International Journal of Nanomedicine* **2014**, *9*, 51.
(41) Ling, H.; Fabbri, M.; Calin, G. A. *Nat. Rev. Drug Discov.* **2013**, *12*, 847.
(42) Anselmo, A. C.; Gupta, V.; Zern, B. J.; Pan, D.; Zakrewsky, M.; Muzykantov, V.; Mitragotri, S. *ACS Nano* **2013**, *7*, 11129.
(43) Whitehead, K. A.; Langer, R.; Anderson, D. G. *Nat. Rev. Drug Discov.* **2009**, *8*, 129.
(44) Mahmoudi, M.; Lynch, I.; Ejtehadi, M. R.; Monopoli, M. P.; Bombelli, F. B.; Laurent, S. *Chem. Rev.* **2011**, *111*, 5610.
(45) Zuckerman, J. E.; Davis, M. E. *Adv. Chronic Kidney Dis.* **2013**, *20*, 500.